ADVANCED FUNCTIONAL MATERIALS

Supporting Information

for *Adv. Funct. Mater.*, DOI: 10.1002/adfm.202000058

Highly Stable Contact Doping in Organic Field Effect Transistors by Dopant-Blockade Method

Youngrok Kim, Katharina Broch, Woocheol Lee, Hebeom Ahn, Jonghoon Lee, Daekyoung Yoo, Junwoo Kim, Seungjun Chung, Henning Sirringhaus, Keehoon Kang, and Takhee Lee**

Supporting Information

Highly stable contact doping in organic field effect transistors by dopant-blockade method

Youngrok Kim, Katharina Broch, Woocheol Lee, Heebeom Ahn, Jonghoon Lee, Daekyoung Yoo, Junwoo Kim, Seungjun Chung, Henning Sirringhaus, Keehoon Kang and Takhee Lee**

Y. Kim, W. Lee, H. Ahn, J. Lee, D. Yoo, J. Kim, Dr. K. Kang, Prof. T. Lee
Department of Physics and Astronomy, and Institute of Applied Physics, Seoul National University, Seoul 08826, Korea

Prof. K. Broch
Institute for applied physics, University of Tuebingen, Auf der Morgenstelle 10, 72076, Tuebingen, Germany

Dr. S. Chung
Photo-Electronic Hybrids Research Center, Korea Institute of Science and Technology, Seoul 02792, Korea

Prof. H. Sirringhaus
Cavendish Laboratory, University of Cambridge, J. J. Thomson Avenue, Cambridge 0HE, UK

*E-mail: keehoon.kang@snu.ac.kr, tlee@snu.ac.kr

Keywords: PBTTT, TCNQ, F_4-TCNQ, solid-state diffusion, contact doping, dopant-blockade

Table of Contents

Section 1. The effect of TNCQ molecules on the electrical properties of the PBTTT OFETs

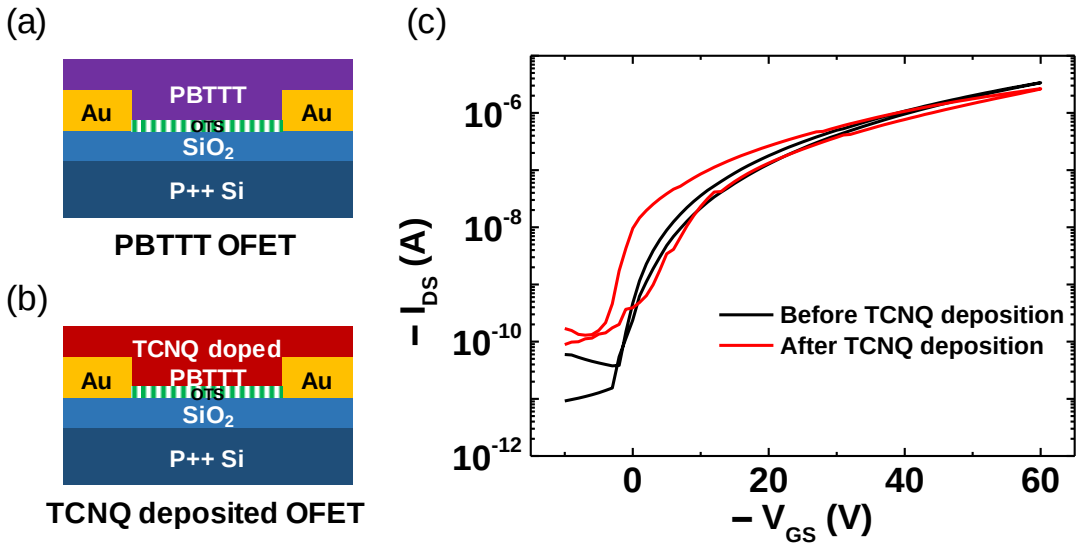

Figure S1. Schematic images of (a) the PBTTT OFET and (b) the PBTTT OFET with TCNQ molecules deposited on the entire PBTTT channel. (c) The transfer curves of the PBTTT OFET (black line) and PBTTT OFET with TCNQ molecules deposited on the entire PBTTT channel (red line).

Section 2. Surface morphology of PBTTT film and DB/DC-FET

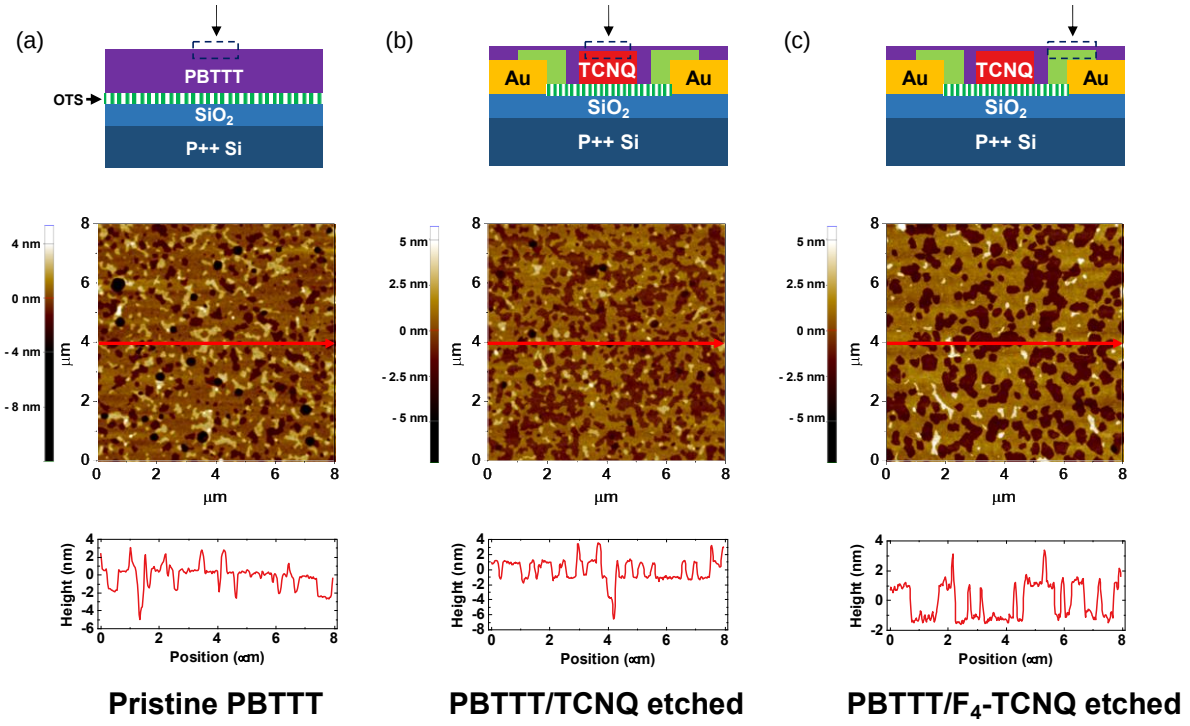

Figure S2. The AFM micrographs (middle) and line-scan profiles (bottom) of (a) a pristine PBTTT film deposited on the OTS-treated SiO_2/Si substrate, (b) TCNQ-incorporated channel region (PBTTT/TCNQ etched) and (c) F_4-TCNQ-doped contact region (PBTTT/F_4-TCNQ etched) in a DB/DC-FET device.

Section 3. Top-view schematic images for DC-FET and DB/DC-FET

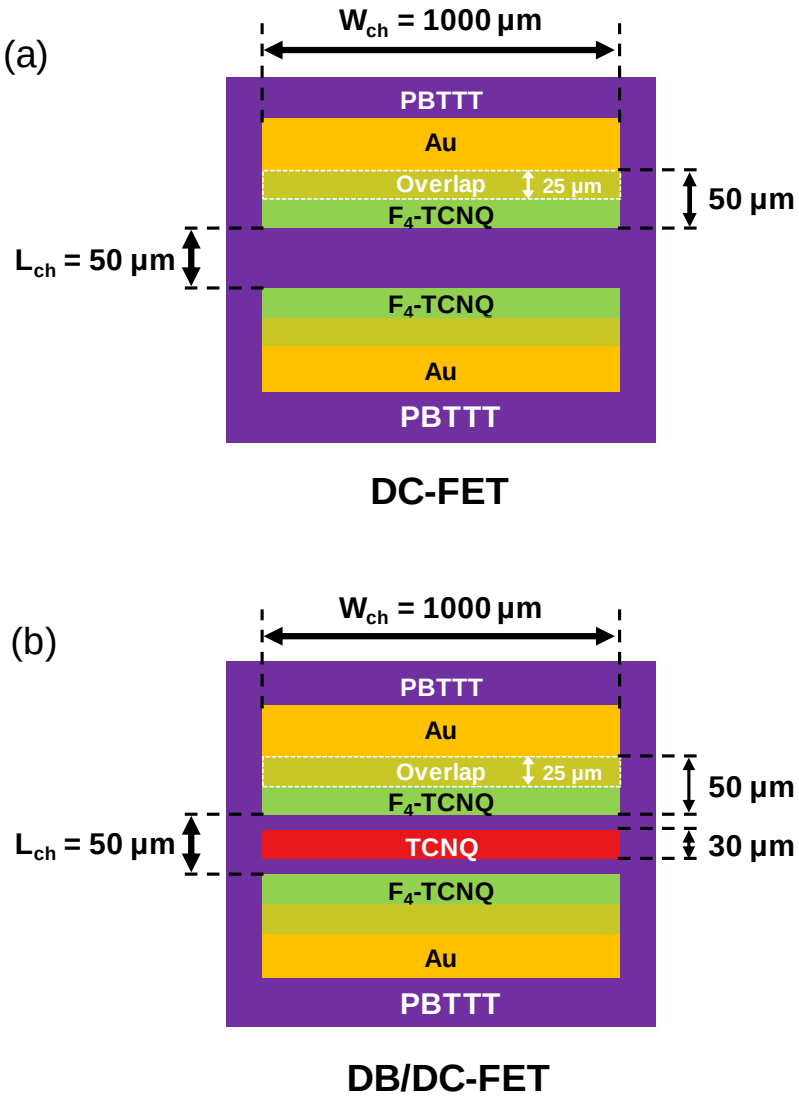

Figure S3. Top-view schematic images of (a) the DC-FET and (b) the DB/DC-FET with the dimensions shown for the effective channel length (L_{ch}) of 50 μm and channel width of 1 mm. The F_4-TCNQ-doped contact region (green and light green), the Au metal contacts (yellow) and TCNQ-incorporated region (red) in the PBTTT (purple) channel region are shown.

Section 4. Comparison of ToF-SIMS depth profile data of cyanide ion

Figure S3 shows the depth profiles of the cyanide ions (CN-) for the pristine PBTTT film and PBTTT/TCNQ film in linear scale. The cyanide ion intensity is consistently higher in the PBTTT/TCNQ film down to the depth of nearly 40 nm which is the thickness of PBTTT film.[S1] The large increases in the depth profiles of the cyanide ion intensity shown at each interface between two different media (i.e. vacuum/PBTTT and PBTTT/SiO_2 interfaces) could be related to the matrix effect.[S2-S4]

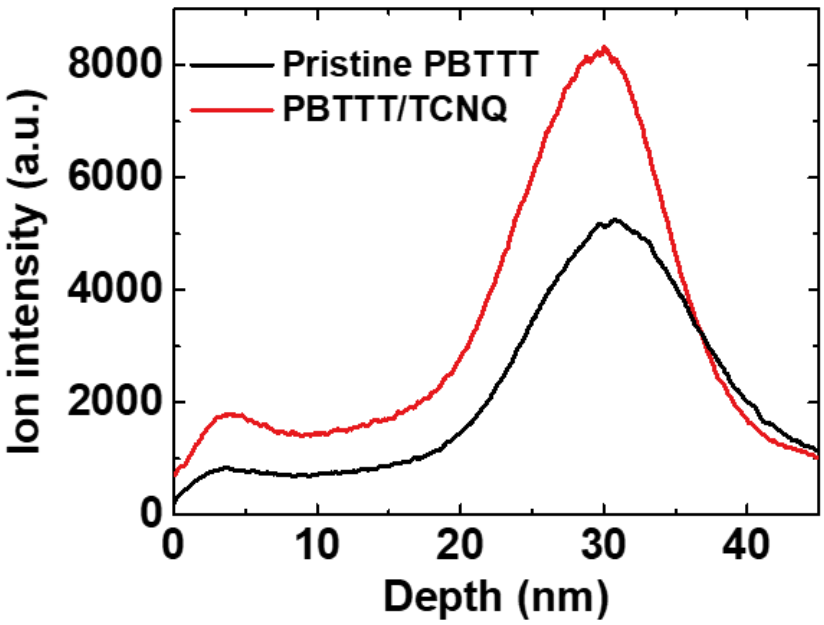

Figure S4. The depth profile of cyanide ion intensity for the pristine PBTTT film (black line) and PBTTT/TCNQ film (red line). The PBTTT/TCNQ film data clearly shows a higher cyanide ion signal than the pristine PBTTT film throughout the entire depth of the PBTTT film.

Section 5. Y-function method for extraction of contact resistance

The Y-function method has been a useful methodology for obtaining the contact resistance of FET devices of organic semiconductors and two-dimensional semiconductors for which the device geometry is usually hard to define. [S5-S8] In order to extract the contact resistance, the Y-function method requires transfer curves (I_{DS}-V_{GS} curve) in a linear regime ($V_{GS} - V_{th} \gg V_{DS}$, where V_{GS}, V_{th} and V_{DS} are gate voltage, threshold voltage and drain-source voltage, respectively). For the DC-FET and DB/DC-FET, I_{DS} could be described as a following equation;

$$I_{DS} = \mu c(V_{GS} - V_{th})V_{DS}(W/L_{eff})$$

$$= \frac{\mu_0 c(V_{GS} - V_{th})V_{DS}(W/L_{eff})}{1 + \alpha(V_{GS} - V_{th})}$$

where μ, μ_0, c, α, W *and* L_{eff} represent the effective mobility, the intrinsic mobility, the capacitance of dielectric layer per unit area, the mobility attenuation factor, the channel width and the effective channel length, respectively. The mobility attenuation factor in the former equation defined as below;

$$\alpha = \alpha_{channel} + \mu_0 c R_{contact}(W/L_{eff}) \approx \mu_0 c R_{contact}(W/L_{eff}) \quad (in\ V_{GS} - V_{th} \gg V_{DS})$$

where $\alpha_{channel}$ and $R_{contact}$ represent the channel contribution on attenuation factor and the contact resistance, respectively.

Y-function is founded by I_{DS} and transconductance (g_m) as the following equation;

$$\mathrm{Y} = \frac{I_{DS}}{\sqrt{g_m}} = \frac{I_{DS}}{\sqrt{(\frac{\partial I_{DS}}{\partial V_{GS}})}} \approx \frac{\frac{\mu_0 c(V_{GS} - V_{th})V_{DS}(W/L_{eff})}{1 + \alpha(V_{GS} - V_{th})}}{\sqrt{\frac{\mu_0 c V_{DS}(W/L_{eff})}{(1 + \alpha(V_{GS} - V_{th}))^2}}} = \sqrt{\mu_0 c V_{DS}(W/L_{eff})}(V_{GS} - V_{th})$$

Then,

$$(\frac{\partial Y}{\partial V_{GS}})^{-1} \times \frac{\partial(1/\sqrt{g_m})}{\partial V_{GS}} \times V_{DS} \approx R_{contact}$$

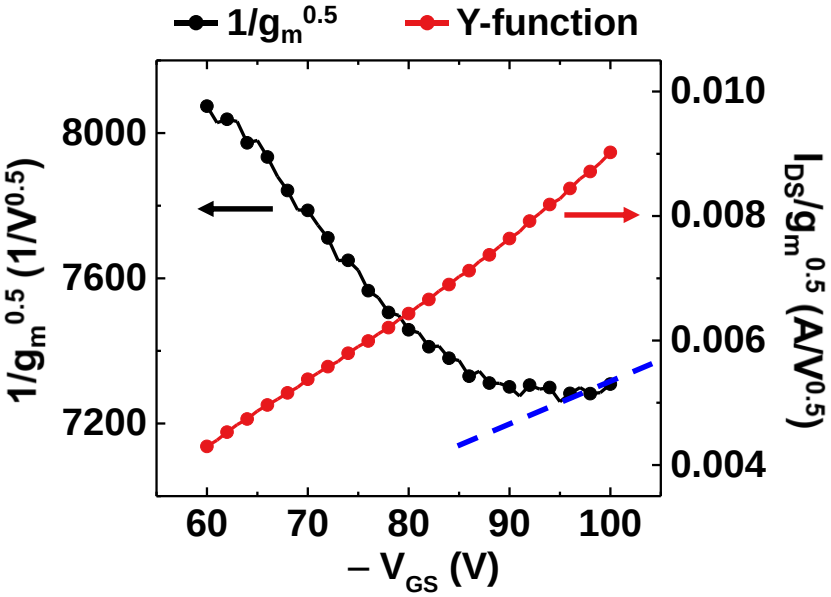

Figure S5. Data for Y-function method; a black line shows $1/\sqrt{g_m}$ (where g_m is the transconductance), a red line is the Y-function and a blue dashed line represents the selected data to extract contact resistance.

Section 6. Time evolution of the transfer curves of the 100 µm channel devices

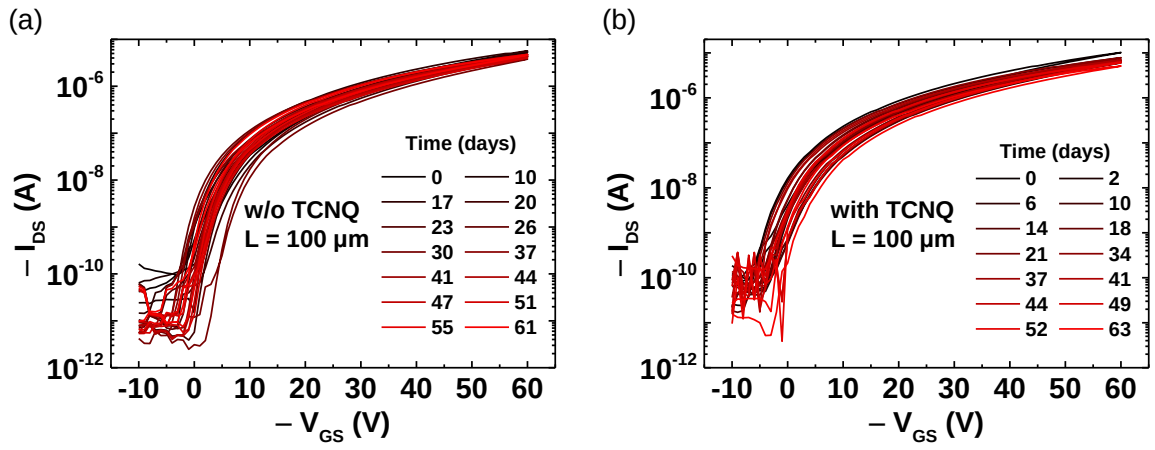

Figure S6. Time evolution of the transfer curves of (a) the DC-FET and (b) the DB/DC-FET with the channel length of 100 µm over two months.

Section 7. Time evolution of the device parameters for the 50 μm channel devices

Both the SS value and the V_{th} of the 50 μm channel DC-FET device show a rapid increase after 20 days which is due to the gradual channel doping via dopant diffusion (Figure S7). This trend agrees well with a rapid decrease of the ON/OFF ratio of the 50 μm channel DC-FET device after 20 days (see Fig 4c in the main manuscript). A similar trend can be seen from the change in the normalized mobility plot (Figure S7c). However, the trend is weaker since the values monotonically decrease for all the devices. The degradation is potentially due to an unintentional, prolonged air exposure during the sample transportation between each measurement. [S9]

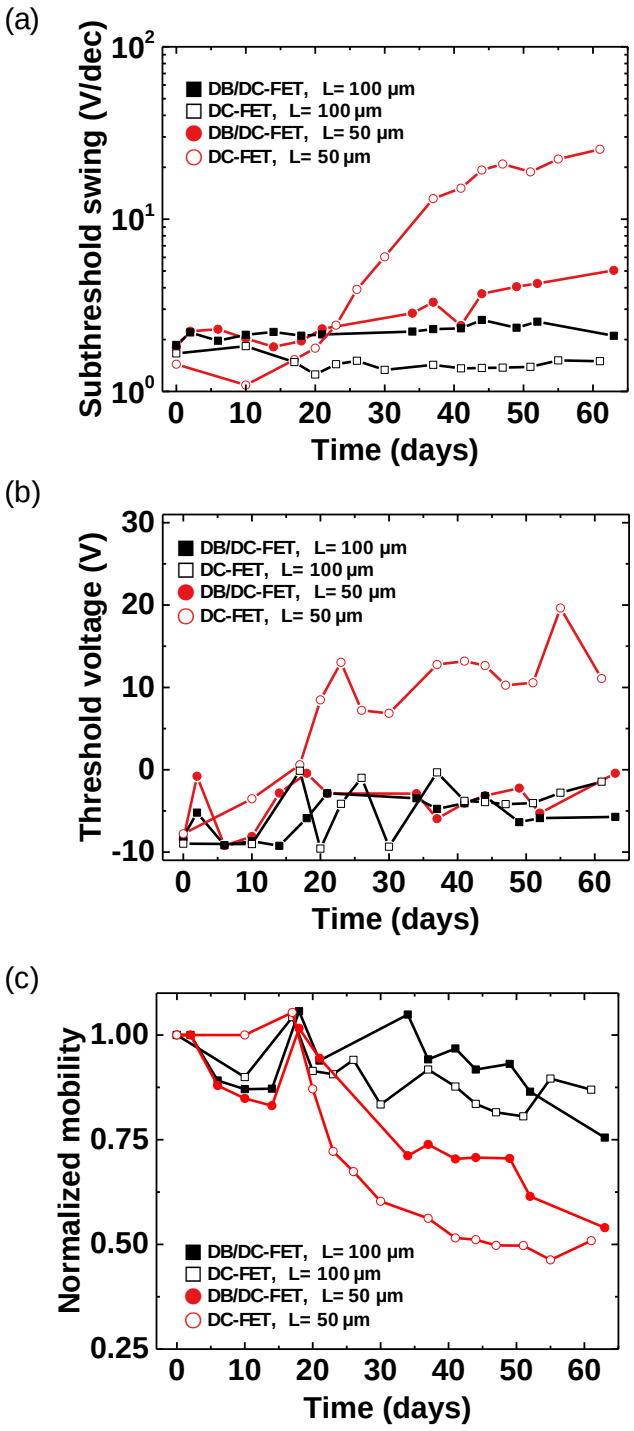

Figure S7. Time evolution of the (a) subthreshold swing, (b) threshold voltage and (c) normalized mobility values for the DC-FET and the DB/DC-FET with the channel length of 50 μm and 100 μm over two months.

Section 8. Drain-voltage-bias-stress effect in DC-FET

The drain-source voltage bias-stress measurement on DC-FET was performed to investigate whether there was any sign of dopant-drift-induced instability. The drain-voltage bias-stress measurement was performed by applying -60 V to the drain. The transfer curves of the pristine and DC-FET devices remain nearly the same after 23 hours of bias-stressing (Figures S8a and S8b). Especially, there is no rise in the OFF current for DC-FET. Therefore, the drift of the dopants induced by the drain bias is unlikely to cause device instability unlike the diffusion-induced device instability.

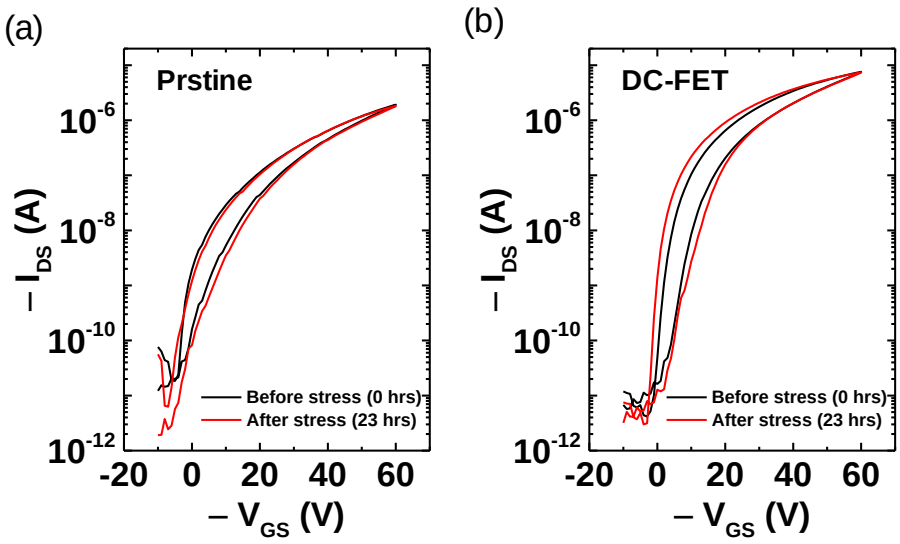

Figure S8. Transfer curves measured before (black) and after (red) the 23 hours of bias-stress test for (a) the pristine FET and (b) DC-FET.

References

[S1] K. Kang, S. Watanabe, K. Broch, A. Sepe, A. Brown, I. Nasrallah, M. Nikolka, Z. Fei, M. Heeney, D. Matsumoto, K. Marumoto, H. Tanaka, S.-i. Kuroda, H. Sirringhaus, *Nat. Mater.* **2016**, 15, 896.

[S2] C. Noël, S. Pescetelli, A. Agresti, A. Franquet, V. Spampinato, A. Felten, A. di Carlo, L. Houssiau, Y. Busby, *Materials* **2019**, 12, 726.

[S3] A. G. Shard, S. J. Spencer, S. A. Smith, R. Havelund, I. S. Gilmore, *Int. J. Mass Spectrom.* **2015**, 377, 599.

[S4] F. M. Green, I. S. Gilmore, M. P. Seah, *Rapid Commun. Mass Spectrom.* **2008**, 22, 4178.

[S5] K. Cho, J. Pak, J.-K. Kim, K. Kang, T.-Y. Kim, J. Shin, B. Y. Choi, S. Chung, T. Lee, *Adv. Mater.* **2018**, 30, 1705540.

[S6] J.-K. Kim, Y. Song, T.-Y. Kim, K. Cho, J. Pak, B. Y. Choi, J. Shin, S. Chung, T. Lee, *Nanotechnology* **2017**, 28, 47LT01.

[S7] Y. Xu, H. Sun, E.-Y. Shin, Y.-F. Lin, W. Li, Y.-Y. Noh, *Adv. Mater.* **2016**, 28, 8531.

[S8] Y. Xu, T. Minari, K. Tsukagoshi, J. A. Chroboczek, G. Ghibaudo, *J. Appl. Phys.* **2010**, 107, 114507.

[S9] I. McCulloch, M. Heeney, C. Bailey, K. Genevicius, I. MacDonald, M. Shkunov, D. Sparrowe, S. Tierney, R. Wagner, W. Zhang, M. Chabinyc, R.. Kline, M. McGehee, M. Toney, *Nat. Mater.* **2006**, 5, 328.